LAWRENCE
LIVERMORE
NATIONAL
LABORATORY

LLNL-JRNL-622841

Nonlinear brightness optimization in Compton scattering

F. V. Hartemann, S. S. Q. Wu

February 27, 2013

Physical Review Letters

Disclaimer

Nonlinear brightness optimization in Compton scattering

Fred V. Hartemann & Sheldon S.Q. Wu

Lawrence Livermore National Laboratory, Livermore, CA 94550

Abstract

In Compton scattering light sources, a laser pulse is scattered by a relativistic electron beam to generate tunable x and gamma rays. Because of the inhomogeneous nature of the incident radiation, the relativistic Lorentz boost of the electrons is modulated by the ponderomotive force during the interaction, leading to intrinsic spectral broadening and brightness limitations. These effects are discussed, along with an optimization strategy to properly balance the laser bandwidth, diffraction, and nonlinear ponderomotive force.

PACS: 07.85.-m, 41.60.Cr, 42.72.-g

Renewed interest in Compton scattering is currently being focused on fundamental QED aspects of the interaction [1] and on advanced technology paths to generate tunable electromagnetic radiation in the x-ray and gamma ray spectral ranges [2].

While the basic physics underlying Compton scattering is well known, a cursory overview of the recent literature on the subject shows that there are still interesting questions related to the nonlinear [3] and radiation reaction [4] regimes, as well as the role and nature of the dressed electron mass during the interaction [5].

The present work focuses on the weakly nonlinear dephasing effect [6] due to the ponderomotive force, and its influence on the maximum differential spectral and angular brightness that can be attained via Compton scattering. In this Letter, we: (1) define a covariant criterion for nonlinear dephasing onset; (2) show the relation between ponderomotive dephasing and total scattering probability; (3) study the balance between bandwidth and diffraction; (4) provide a strategy for nonlinear optimization, including bandwidth, diffraction, and nonlinear dephasing.

QED units are used throughout: length, mass, time, and charge are measured in units of $\lambda\!\!\!^{-} = \hbar / m_0 c$, m_0, $\lambda\!\!\!^{-} / c$, and e, respectively. In these units, the permittivity of vacuum is $\varepsilon_0 = 1/4\pi\alpha$. We consider a relativistic electron interacting with a polychromatic plane wave described by the 4-potential: $A_\mu = \sigma_\mu A(\phi)$; $\phi = k_\mu x^\mu$, $\sigma_\mu \sigma^\mu = -1$. In the Lorentz gauge, $\partial_\mu A^\mu = 0 = k_\mu \sigma^\mu A'(\phi)$; and the Lorentz force equation can be solved exactly to obtain the electron nonlinear 4-velocity [7]:

$$u_\mu = u_\mu^0 - A_\mu - k_\mu \frac{A_\nu \left(A^\nu - 2u_0^\nu \right)}{2k_\lambda u_0^\lambda} = u_\mu^0 - \varepsilon_\mu A(\phi) + k_\mu \frac{A^2(\phi)}{2k_\lambda u_0^\lambda}, \tag{1}$$

where $\varepsilon_\mu = \sigma_\mu - k_\mu \sigma_\nu u_0^\nu / k_\lambda u_0^\lambda$. The first term is the initial ballistic electron velocity; the term linear in $A(\phi)$ contains the electric and magnetic coupling to the incident wave; the quadratic term corresponds to the ponderomotive force, which couples the transverse electron oscillation to its axial dynamics via the transverse magnetic field.

In cases where the recoil parameter, $\mu = k_\mu q^\mu$, remains small, and spin can be ignored, the brightness is adequately described by the classical radiation formula [8]:

$$\frac{d^2N}{dqd\Omega} = \frac{\alpha q}{4\pi^2}\left|\pi^\mu \int_{-\infty}^{+\infty} u_\mu e^{iq_\nu x^\nu}\, d\tau\right|^2 . \tag{2}$$

Here, q_μ is the scattered radiation 4-wavenumber; π_μ is its 4-polarization; and $x_\mu(\tau)$ is the electron 4-trajectory, parameterized by the proper time, τ.

For a plane wave of constant amplitude, $A(\phi) = A_0 \cos\phi$, the electron 4-velocity is integrated to yield the 4-position:

$$x_\mu(\phi) = x_\mu^0 + \int_0^\phi \frac{dx_\mu}{d\tau}\frac{d\tau}{d\varphi}d\varphi = x_\mu^0 + u_\mu^0 \frac{\phi}{\kappa} - \varepsilon_\mu \frac{A_0}{\kappa}\sin\phi + k_\mu \frac{A_0^2}{8\kappa^2}(2\phi + \sin 2\phi). \tag{3}$$

$\kappa = k_\mu u_0^\mu = d\phi / d\tau$ is the incident light-cone variable and x_μ^0 is the initial 4-position.

Combining Eqs. (2) and (3) in the weak field limit ($A_0 \ll 1$), we have:

$$\frac{d^2N}{dqd\Omega} \simeq \frac{\alpha q A_0^2}{4\pi^2\kappa^2}\left|\pi^\mu \int_{-\infty}^{+\infty}\left(\varepsilon_\mu \cos\phi + iu_\mu \frac{q_\nu \varepsilon^\nu}{\kappa}\sin\phi\right) e^{iq_\nu\left(\frac{u^\nu}{\kappa} + k^\nu \frac{A_0^2}{4\kappa^2}\right)\phi} d\phi\right|^2 . \tag{4}$$

Here, we have used $e^z \simeq 1 + z$; and neglected quadratic terms in A_0, except for the 2nd harmonic in the radiation phase. For conciseness, the initial 4-velocity now reads u_μ.

The single electron coherence factor [9] is one. For a square pulse, the integral is performed to yield:

$$\frac{d^2N}{dqd\Omega} \simeq \frac{\alpha q A_0^2 \Delta\phi^2}{16\pi^2\kappa^2}\left|\sum_{\pm}\left(\varepsilon_\mu \pm u_\mu \frac{q_\nu \varepsilon^\nu}{\kappa}\right)\mathrm{sinc}\left\{\frac{\Delta\phi}{2}\left[1\pm\left(\frac{\lambda}{\kappa}+\mu\frac{A_0^2}{4\kappa^2}\right)\right]\right\}\right|^2; \qquad (5)$$

$\lambda = q_\mu u^\mu$ is the scattered light-cone variable and $\Delta\phi$ is the duration of the pulse.

The primary peak corresponds to a null argument, while the first zero is obtained when the argument is equal to $\pm\pi$; we can then quantify the onset of significant ponderomotive dephasing as described in Fig. 1: starting from the linear case, where $A_0 \to 0$, we find the Doppler shift condition, $\kappa - \lambda = 0$; for non-zero amplitude, the primary peak is downshifted and the first zero is located at $\frac{\Delta\phi}{\kappa}\left(\kappa - \lambda - \frac{\mu}{4\kappa}A_0^2\right) = \pi$. We define the ponderomotive dephasing onset condition as: $\frac{\mu}{4\kappa^2}A_0^2\Delta\phi = \pi = \Lambda A_0^2\Delta\phi$, where Λ is a geometrical factor. For head-on collisions, and on-axis radiation, $\Lambda = 1/2$, and the onset condition for ponderomotive dephasing is simply: $A_0^2\Delta\phi = 2\pi$.

In the more general case of an arbitrary incident plane wave, we have:

$$\frac{d^2N}{dqd\Omega} \simeq \frac{\alpha q}{4\pi^2\kappa^2}\left|\pi^\mu \int_{-\infty}^{+\infty}\left[\varepsilon_\mu A(\phi) + iu_\mu \frac{q_\nu\varepsilon^\nu}{\kappa}\int_0^\phi A(\varphi)d\varphi\right]e^{i\left[\frac{\lambda}{\kappa}\phi+\frac{\mu}{2\kappa^2}\int_0^\phi \overline{A^2(\varphi)}d\varphi\right]}d\phi\right|. \qquad (6)$$

The weakly nonlinear dephasing term, averaged over an optical cycle, plays an important role because it can result in a significant accumulated phase shift for sufficiently long pulses. In fact, this term is directly related to the total radiation probability, $N = \int \sigma j_\mu \Phi^\mu d^4x$; where $\sigma = 8\pi\alpha^2/3$ is the total scattering cross-section; $j_\mu = n_e u_\mu/\gamma$ is the electron 4-current density; and $\Phi_\mu = n_\lambda k_\mu / k$ is the incident photon

4-flux; n_e and n_λ are the respective electron and photon number densities. In the case of a single electron, $N = \sigma \int n_\lambda(t) \frac{\kappa}{\gamma k} dt = \sigma \int n_\lambda(\phi) d\phi / k$. The incident photon density is derived from the electromagnetic energy density: $n_\lambda = \overline{\mathbf{E}^2} / 4\pi\alpha k$. Combining these results, we obtain: $N = \frac{2}{3}\alpha \int \overline{A'^2}\, d\phi$. Comparing this expression with Eq. (6), we see that, in the case of a slow-varying envelope, where $A(\phi) = \frac{1}{2} A_0 g(\phi) \exp(-i\phi) + \text{c.c.}$ and $|g'/g| \ll 1$, the total phase shift due to the ponderomotive force is indeed proportional to the total scattering probability: $\frac{\mu}{2\kappa^2} \int_{-\infty}^{+\infty} \overline{A^2}\, d\phi \simeq \frac{\mu A_0^2}{4\kappa^2} \int_{-\infty}^{+\infty} |g(\phi)|^2 d\phi$; and $N \simeq \frac{\alpha}{3} A_0^2 \int_{-\infty}^{+\infty} |g(\phi)|^2 d\phi$.

Continuing with the slow-varying envelope approximation, the radiation formula reads:

$$\frac{d^2N}{dq d\Omega} \simeq \frac{\alpha q A_0^2}{16\pi^2\kappa^2} \left| \pi^\mu \left(\varepsilon_\mu + u_\mu \frac{q_\nu \varepsilon^\nu}{\kappa} \right) \int_{-\infty}^{+\infty} g(\phi) e^{-i\left(1-\frac{\lambda}{\kappa}\right)\phi} e^{i\omega \int_0^\phi |g(\varphi)|^2 d\varphi} d\phi \right|^2 ; \qquad (7)$$

where $\omega = \mu A_0^2 / 4\kappa^2$.

Assuming that the Fourier transform of *g* is known, and defining

$$w(\phi) = e^{i\omega \int_0^\phi g^2(\varphi) d\varphi} = \frac{1}{\sqrt{2\pi}} \int_{-\infty}^{+\infty} \tilde{w}(\theta) e^{-i\theta\phi} d\theta; \quad \tilde{w}(\theta) = \frac{1}{\sqrt{2\pi}} \int_{-\infty}^{+\infty} w(\phi) e^{i\theta\phi} d\phi; \qquad (8)$$

we have, by direct application of the convolution theorem:

$$\int_{-\infty}^{+\infty} g(\phi) e^{-i\phi\left(1-\frac{\lambda}{\kappa}\right)} e^{i\omega \int_0^\phi g^2(\varphi) d\varphi} d\phi = \sqrt{2\pi} \int_{-\infty}^{+\infty} \tilde{w}(\theta) \tilde{g}\left(\frac{\lambda}{\kappa} - 1 - \theta \right) d\theta. \qquad (9)$$

$w(\phi)$ can be approximated by a simple ramp model, as illustrated in Fig. 2; then:

$$\tilde{w}(\theta) = \sqrt{\frac{2}{\pi}} \left(\frac{1}{\omega+\theta} - \frac{1}{\theta} \right) \sin\left[(\omega+\theta) \tfrac{\delta\phi}{2} \right] + \frac{1}{\sqrt{2\pi}} \cos\left(\omega \tfrac{\delta\phi}{2} \right) \delta(\theta). \qquad (10)$$

The role of the total ponderomotive dephasing in terms of spectral modulation is encapsulated in the $\cos\left(\frac{\omega\delta\phi}{2}\right)$ modulation term.

To validate this approximation, consider a Gaussian pulse, $g(\phi)=e^{-\phi^2/\Delta\phi^2}$, as illustrated in Fig. 2, where the exact and approximate spectra are shown to be in reasonable agreement, confirming that the key parameter is the nonlinear dephasing accumulated over the entire interaction, $\varpi=\frac{A_0^2\mu}{4\kappa^2}\int_{-\infty}^{+\infty}\left|g\left(\phi\right)\right|^2 d\phi$. This is the sought-after criterion for resolving the weakly nonlinear dephasing onset: for long pulses, the spectrum is narrow, and a small downshift is sufficient to significantly alter the spectrum; conversely, shorter pulses require more ponderomotive downshift to resolve the effect. The Lorentz invariant quantity ϖ provides the scale for this mechanism. The main spectral peak is downshifted by $1/\left(1+\overline{A^2}\right)$, and the number of satellite lines scales roughly as $n=\varpi/2\pi$. Finally, setting $\varpi\le 2\pi$ for linear interactions translates into $N\lesssim\frac{4\pi}{3}\alpha\approx 3\%$.

We now address the fully three-dimensional case. Working within the context of the paraxial approximation [10], for a linearly polarized, cylindrically symmetric Gaussian transverse distribution at focus, the transverse potential takes the form: $A_x=\frac{1}{2}A_0 g\left(\phi\right)e^{i\phi-\bar{r}^2/\left(1-i\bar{z}\right)}/\left(1-i\bar{z}\right)+\text{c.c.}$. Here, $\phi=k_0\left(t+z\right)$ is the phase of the wave; $z_0=\frac{1}{2}k_0 w_0^2$ is the Rayleigh length, expressed in terms of the focal waist, w_0, and axial wavenumber, k_0; $\bar{z}=z/z_0$; and $\bar{r}=r/w_0$. For an on-axis electron, the axial position as a function of phase is easily derived; the ballistic component is simply: $dz/d\phi=u_z/\kappa\simeq e^{-\rho}\sinh\rho/k_0$; ρ is the rapidity. If our reference electron is

synchronized, and in the ultra-relativistic case, where $e^{-\rho}\sinh\rho \simeq \frac{1}{2}$, the potential along the ballistic trajectory is: $A_x\left[\overline{r}=0, z(\phi), \phi\right] \simeq \frac{1}{2}A_0 g(\phi) e^{-i\phi} / \left(1 - i\frac{\phi}{k_0^2 w_0^2}\right) + \text{c.c.}$. The pulse energy is evaluated by integrating the Poynting flux through the focal plane over the pulse duration. Using $x = \phi / \Delta\phi$; and taking into account $\left|g'/g\right| \ll 1$:

$$W_0 \simeq \frac{A_0^2 \Delta\phi k_0^2 w_0^2}{16\alpha} \int_{-\infty}^{+\infty} g^2(x)\,dx = \overline{W}_0 \int_{-\infty}^{+\infty} g^2(x)\,dx. \tag{11}$$

Since the maximum spectral density is radiated on-axis, we specialize our analysis to that situation, and for head-on collisions; the radiation phase is: $q_\mu x^\mu \simeq q e^{-2\rho}\phi / k_0 = \chi\phi$.

The linear radiation integral reads:

$$\frac{d^2N}{dq d\Omega} = \frac{\alpha^2}{\pi^2}\overline{W}_0 \eta^2 \chi \left| \int_{-\infty}^{+\infty} \frac{g(x)}{1 - i\eta^2 x} e^{-ix\Delta\phi(1-\chi)}\,dx \right|^2. \tag{12}$$

Here, we have introduced the normalized Doppler-shifted frequency, $\chi = q e^{-2\rho} / k_0$; the scale parameter $\eta = \sqrt{\Delta\phi} / k_0 w_0$, which measures the balance between bandwidth and diffraction; and used the normalized incident pulse energy. For illustration, consider the case of a Gaussian temporal envelope:

$$\frac{d^2N}{dq d\Omega} = 4\pi^2\alpha^2 \overline{W}_0 \frac{\chi}{\eta^2} \exp\left[\frac{2}{\eta^4} + \frac{2\Delta\phi}{\eta^2}(\chi - 1)\right] \Phi^2\left[\frac{1}{\eta^2} + \frac{\Delta\phi}{2}(\chi - 1)\right]. \tag{13}$$

This is the convolution product of the Fourier transforms of a Gaussian and a Lorentzian; Φ is the complementary error function [11]. Rescaling the frequency as $\overline{\chi} = \frac{1}{\eta^2} + \frac{\Delta\phi}{2}(\chi - 1)$, for large values of $\Delta\phi$, we have: $S_0 \simeq 4\alpha^2 \overline{W}_0 \eta^{-2} e^{-2/\eta^4} e^{4\overline{\chi}/\eta^2} \Phi^2(\overline{\chi})$. The form factor, $f_{\Delta\phi} = S_0\left[\chi^*(\eta), \eta; \Delta\phi\right] / 4\alpha^2 \overline{W}_0$, is a strong function of η that also weakly

depends on $\Delta\phi$, as illustrated in Fig. 3; and shows a clear maximum, $f_\infty\left(\eta^*\right) \simeq 3.15379$, at $\eta^* \simeq 1.71024$, and $\bar{\chi}^*\left(\eta^*\right) \simeq -0.389338$.

Physically, this is significant, as it shows that for a fixed incident laser pulse energy, the maximum number of photons scattered per unit solid angle and frequency is obtained when the transverse and axial scales are matched: $\sqrt{\Delta\phi} = \eta^* k_0 w_0$; bandwidth and diffraction are balanced. This condition is independent of the normalized potential: longer pulses diffracting slower will yield the same peak spectral density as long as the matching condition is satisfied. Finally, it is noteworthy that, while the details of this linear optimum depend on the exact pulse shape, the approach is quite general.

For a self-consistent analysis, the effects of nonlinear dephasing are now included. Proceeding exactly as before, the radiation integral with nonlinear dephasing is derived by considering the 2nd harmonic axial position modulation driven by the ponderomotive force: $u_z\left(\bar{r}=0,\phi\right) \simeq \sinh\rho + \frac{k_0}{2\kappa} A_0^2 \left\{ \frac{1}{2} g\left(\phi\right) e^{-i\phi} / \left[1 - i\bar{z}\left(\phi\right)\right] + \text{c.c.} \right\}$. The spectral density from Eq. (7) can be recast as follows:

$$\frac{d^2N}{dqd\Omega} = \frac{\alpha}{16\pi^2} \frac{A_0^2 \Delta\phi^2}{k_0} \chi \left| \int_{-\infty}^{+\infty} \frac{g\left(x\right)}{1 - i\eta^2 x} e^{-ix\Delta\phi\left(1-\chi\right)} e^{i\chi \frac{A_0^2\Delta\phi}{2} \int_0^x \frac{g^2(y)}{1+\eta^4 y^2} dy} \, dx \right|^2 . \qquad (14)$$

To study the interplay between bandwidth, diffraction, and weakly nonlinear effects, consider a Gaussian temporal envelope: $g\left(x\right) = e^{-x^2}$. We start from a linear spectrum with fixed bandwidth, $\Delta\phi^{-1}$; and matched in terms of diffraction: $\eta = \eta^*$. The ponderomotive dephasing, $\delta = A_0^2 \Delta\phi / 2$, is then varied to generate nonlinear spectra, as shown in Fig. 4 (top). This is equivalent to varying the incident pulse energy. For each

spectrum, the maximum value of the main spectral line is determined, and plotted as a function of incident pulse energy on Fig. 4 (middle); for two different incident pulse durations corresponding to CPA (ps) and non-CPA (ns) laser technologies, respectively; and for three values of η. The (linear) matched beam produces the highest brightness, which scales very nearly linearly with the incident energy: higher energy allows one to use longer pulses and softer foci, which yield the best performance for our optimization metric. The most interesting conclusion is that the brightness degrades as one enters the nonlinear regime. Physically, this can be understood as follows: the nonlinear dephasing simply redistributes the scattered energy into parasitic channels, without increasing the main spectral line. Mathematically, Parseval's theorem indicates that, because the Fourier transform is multiplied by a phase factor of modulus one, we have:

$$\left|\int_{-\infty}^{+\infty}\int_{-\infty}^{+\infty}\frac{g(x)}{1-i\eta^2 x}e^{-ix\Delta\phi(1-\chi)}e^{i\chi\frac{A_0^2\Delta\phi}{2}\int_0^x\frac{g^2(y)}{1+\eta^4y^2}dy}\,dx\,d\chi\right|^2=\left|\int_{-\infty}^{+\infty}\int_{-\infty}^{+\infty}\frac{g(x)}{1-i\eta^2 x}e^{-ix\Delta\phi(1-\chi)}\,dx\,d\chi\right|^2. \qquad (15)$$

Finally, the maximum on-axis spectral and angular scattered photon number density, in units of photons per 0.1% bandwidth per mrad^2, for a balanced Gaussian-Lorentzian beam is determined as follows: we first define

$$B_x=\frac{d^2N}{dqd\Omega}\Delta q\Delta\Omega=\frac{\alpha}{4\pi^2}e^{2\rho}A_0^2\Delta\phi^2\chi^2h\left(\eta,\Delta\phi,\chi,A_0\right)\times10^{-9};$$
$$h=\left|\int_{-\infty}^{+\infty}\frac{e^{-x^2-ix\Delta\phi(1-\chi)}}{1-i\eta^2x}e^{i\chi\frac{A_0^2\Delta\phi}{2}\int_0^x\frac{e^{-2y^2}}{1+\eta^4y^2}dy}\,dx\right|^2. \qquad (16)$$

Here $\Delta q=q\times10^{-3}$, and $\Delta\Omega=10^{-6}$. Next, for a fixed value of $\Delta\phi$, the brightness triple maximum is located numerically: $\partial_{A_0}\partial_\chi\partial_\eta\left[A_0^{*2}\chi^{*2}h\left(\eta^*,\Delta\phi,\chi^*,A_0^*\right)\right]=0$. The corresponding

brightness is $B_x^* \simeq \frac{\alpha}{4\pi^2} A_0^{*2} \Delta\phi^2 e^{2\rho} \times 10^{-9} \times 0.241115$; with $\frac{A_0^{*2}\Delta\phi}{2} \int_{-\infty}^{+\infty} \frac{e^{-2x^2}}{1+\eta^{*4}x^2} dx = 2.704 \times 2\pi$.

The incident pulse duration is $\Delta\phi / k_0$; the focal spot radius is $w_0 = \sqrt{\Delta\phi} / k_0 \eta^*$; and the energy is $W_0 = \sqrt{\frac{\pi}{2}} A_0^{*2} \Delta\phi^2 / \left(16\alpha k_0 \eta^{*2}\right)$. We see that all parameters are governed by a single variable, which can be chosen as $W_0 \propto \Delta\phi$, as shown in Fig. 4 (bottom).

In conclusion, we have studied the linear and nonlinear optimization of the on-axis spectral angular brightness for single, synchronized, on-axis electron interacting with a laser pulse, under the following conditions: Gaussian cylindrical focal distribution, slow-varying temporal envelope, and linear polarization. The maximum brightness is obtained when pulse duration and diffraction are balanced, and one operates near the onset of the weakly nonlinear ponderomotive dephasing. Within this context, larger incident laser pulse energy allows for narrower bandwidth and softer foci, yielding a linear increase in brightness. We also note that these effects can be minimized if the ponderomotive force remains constant along the electron trajectories; however, such an interaction geometry would require that the laser pulse duration and focal radius be much larger than the temporal and spatial scales characterizing the electron bunch, at a prohibitive energy cost. Additionally, the spatial and temporal shaping required becomes increasingly difficult at higher pulse energies.

Acknowledgements

This work was performed under the auspices of the U.S. Department of Energy by Lawrence Livermore National Laboratory under Contract DE-AC52-07NA27344, and

under LLNL 12ERD057. F.V. Hartemann would also like to acknowledge useful conversations with D.T. Santa Maria.

References

[1] A. Di Piazza, Rev. Mod. Phys. 84, 1177 (2012), and references therein.

[2] D.J. Gibson *et al*., Phys. Plasmas 11, 2857 (2004); W.J. Brown *et* al., Phys. Rev. ST Accel. Beams 7, 060702 (2004); D.J. Gibson *et al*., Phys. Rev. ST Accel. Beams. 13, 070703 (2010); F.V. Hartemann *et al*., Phys. Rev. ST Accel. Beams 8, 100702 (2005).

[3] T. Heinzl, D. Seipt, and B. Kämpfer, Phys. Rev. A 81, 022125 (2010); D. Seipt and B. Kämpfer, Phys. Rev. A 83, 022101 (2011); F. Mackenroth and A. Di Piazza, Phys. Rev. A 83, 032106 (2011); D. Seipt and B. Kämpfer, Phys. Rev. ST Accel. Beams 14, 040704 (2011); F. Mackenroth and A. Di Piazza, Phys. Rev. Lett. 110, 070402 (2013).

[4] A. Di Piazza, K. Z. Hatsagortsyan, and C. H. Keitel, Phys. Rev. Lett. 102, 254802 (2009); A. Di Piazza, K. Z. Hatsagortsyan, and C. H. Keitel, Phys. Rev. Lett. 105, 220403 (2010).

[5] Chris Harvey *et al*., Phys. Rev. Lett. 109, 100402 (2012).

[6] F.V. Hartemann *et al*., Phys. Rev. Lett. 105, 130801 (2010).

[7] J.W. Meyer, Phys. Rev. D 3, 621 (1971).

[8] *High-Field Electrodynamics*, F.V. Hartemann, CRC Press, ISBN 0-8493-2378-9 (2002).

[9] F.V. Hartemann, Phys. Rev. E 61, 972 (2000).

[10] F.V. Hartemann *et al*., Phys. Rev. E 54, 2956 (1996).

[11] *Tables of Integrals, Series, and Products*, I.S. Gradshteyn and I.M. Ryzhik, Academic Press, ISBN 0-12-294760-6 (1980).

[12] F.V. Hartemann *et al*., Phys. Rev. E 58, 5001 (1998).

Figure captions

Fig. 1 Quadratic sinc spectra in the linear limit and with nonlinear dephasing.

Fig. 2 Top: schematic representation of the ramp approximation of the nonlinear dephasing. Bottom: nonlinear spectra evaluated numerically and using the ramp approximation for 2 different values of $\varpi = \frac{A_0^2 \mu}{4\kappa^2} \int_{-\infty i}^{+\infty} g^2 \, d\phi$. The spectra are normalized for comparison; in particular, the co-factor $\frac{\alpha q A_0^2}{16\pi^2\kappa^2}$ is omitted.

Fig. 3 Top: linear spectra of a Gaussian-Lorentzian pulse for different balances between bandwidth and diffraction. Bottom: following the maximum angular and spectral brightness as function of $\eta = \sqrt{\Delta\phi} / k_0 w_0$, for a fixed total energy, in the linear regime.

Fig. 4 Top: nonlinear spectra for $\Delta\phi = 10^5$, and $\eta = 1.7087$; the spectra are divided by $\alpha^2 \overline{W_0} / \pi^2$ for comparison. Middle: following the maximum brightness as a function of W_0 for $\Delta\phi = 10^3$ (dashed) and $\Delta\phi = 10^6$ (solid), and 3 values of η. The energy and brightness scales correspond to the long pulse; they have to be multiplied by 10^{-3} for the short pulse. Bottom: optimized nonlinear Gaussian-Lorentzian parameters as function of available laser energy: A_0^{*2} (dashed); w_0 (dotted); Δt (dashed-dotted); and B_x^* (solid), for $\rho = 7.6009$ ($\gamma = 10^3$).

Figure 1

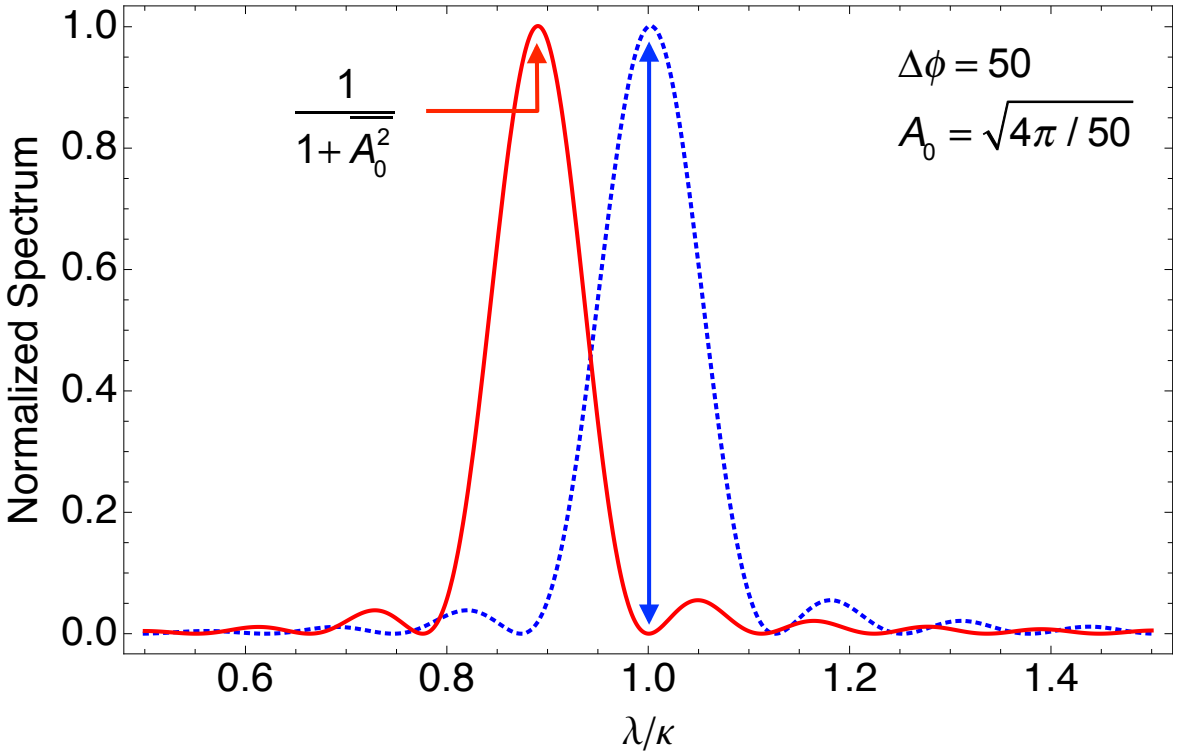
Normalized Spectrum
1.0
0.8
0.6
0.4
0.2
0.0
0.6
0.8
1.0
1.2
1.4
λ/κ
1
1+A0^2
Δφ = 50
A0 = √(4π / 50)

Figure 2

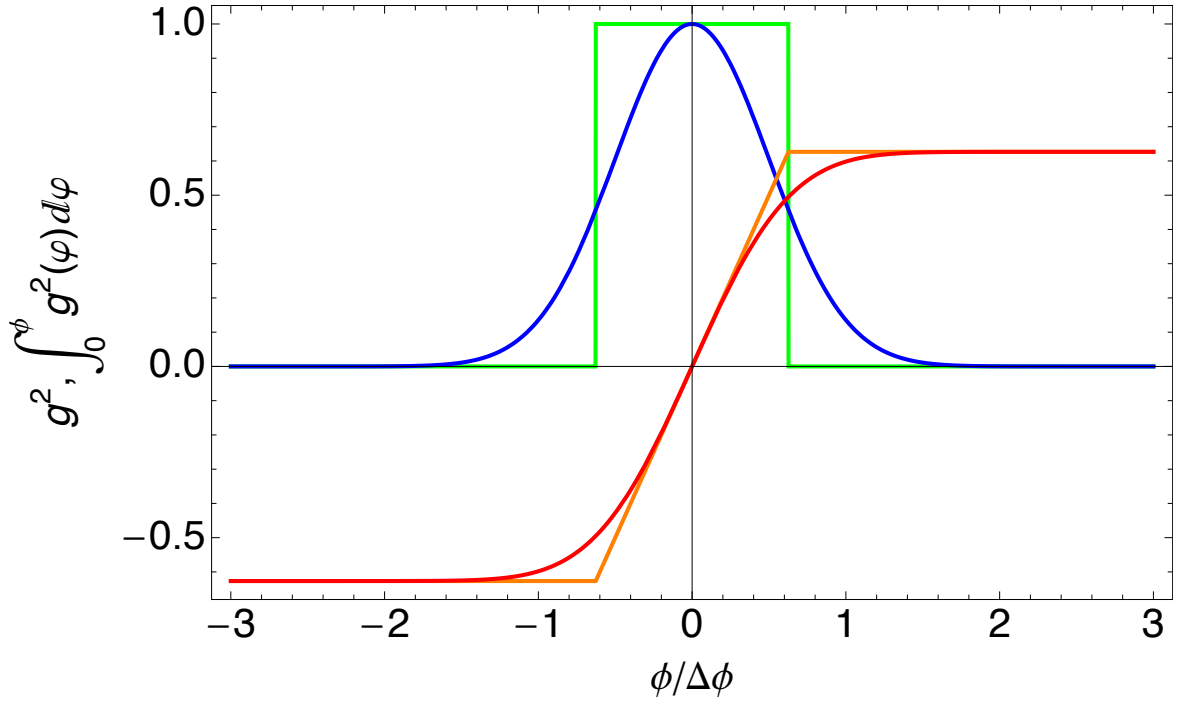
1.0
0.5
0.0
−0.5
−3
−2
−1
0
1
2
3
$g^2, \int_0^\phi g^2(\varphi)d\varphi$
$\phi/\Delta\phi$

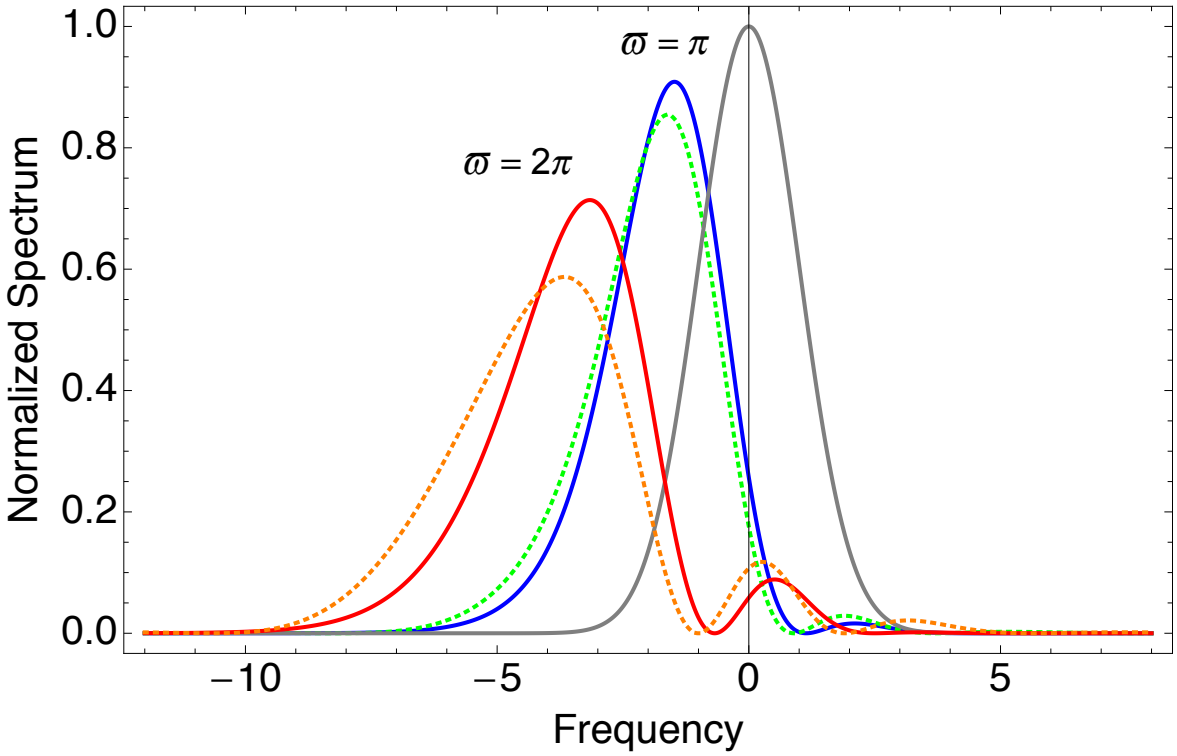
1.0
0.8
0.6
0.4
0.2
0.0
−10
−5
0
5
Normalized Spectrum
Frequency
$\varpi = \pi$
$\varpi = 2\pi$

Figure 3

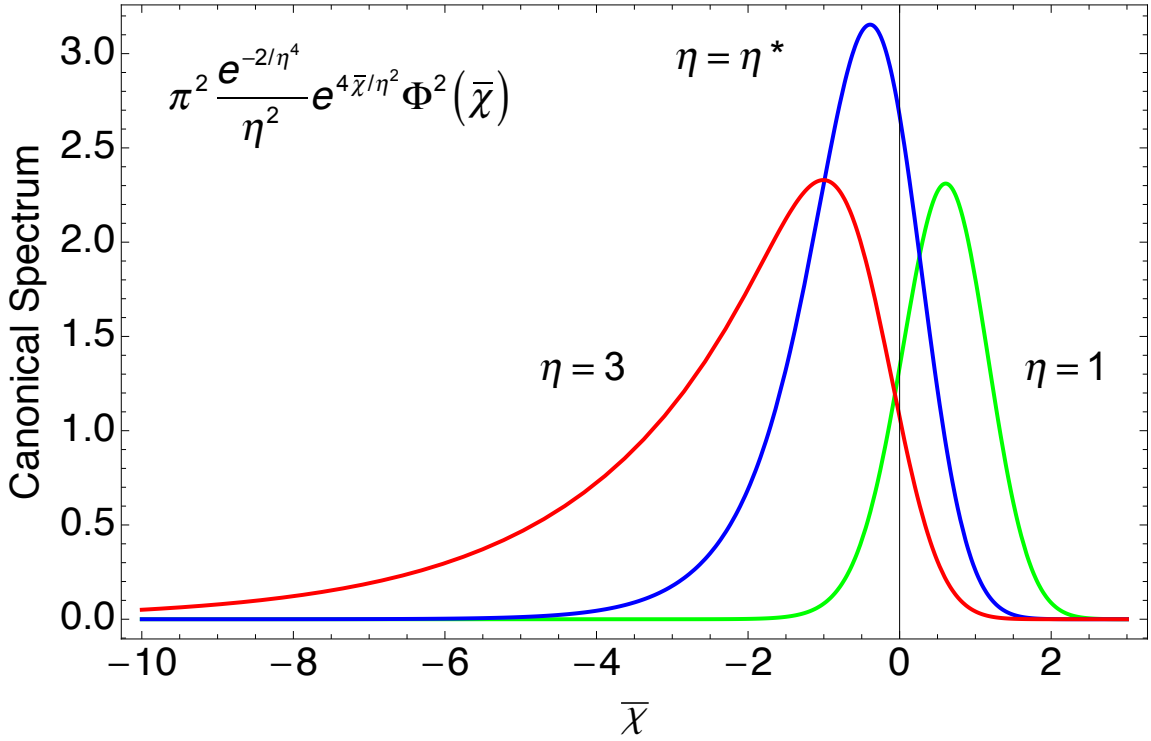
$\pi^2 \frac{e^{-2/\eta^4}}{\eta^2} e^{4\bar{\chi}/\eta^2} \Phi^2(\bar{\chi})$
$\eta = \eta^*$
$\eta = 3$
$\eta = 1$
Canonical Spectrum
$\bar{\chi}$

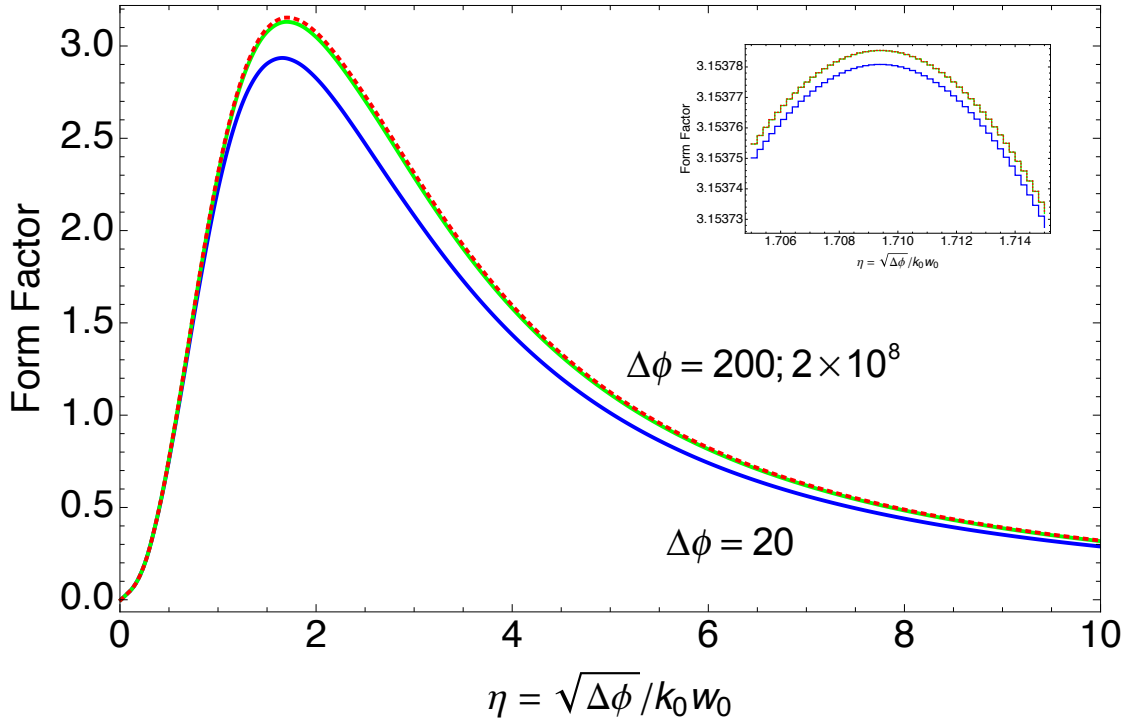
Form Factor
$\Delta\phi = 200; 2\times10^8$
$\Delta\phi = 20$
$\eta = \sqrt{\Delta\phi}/k_0 w_0$

Figure 4

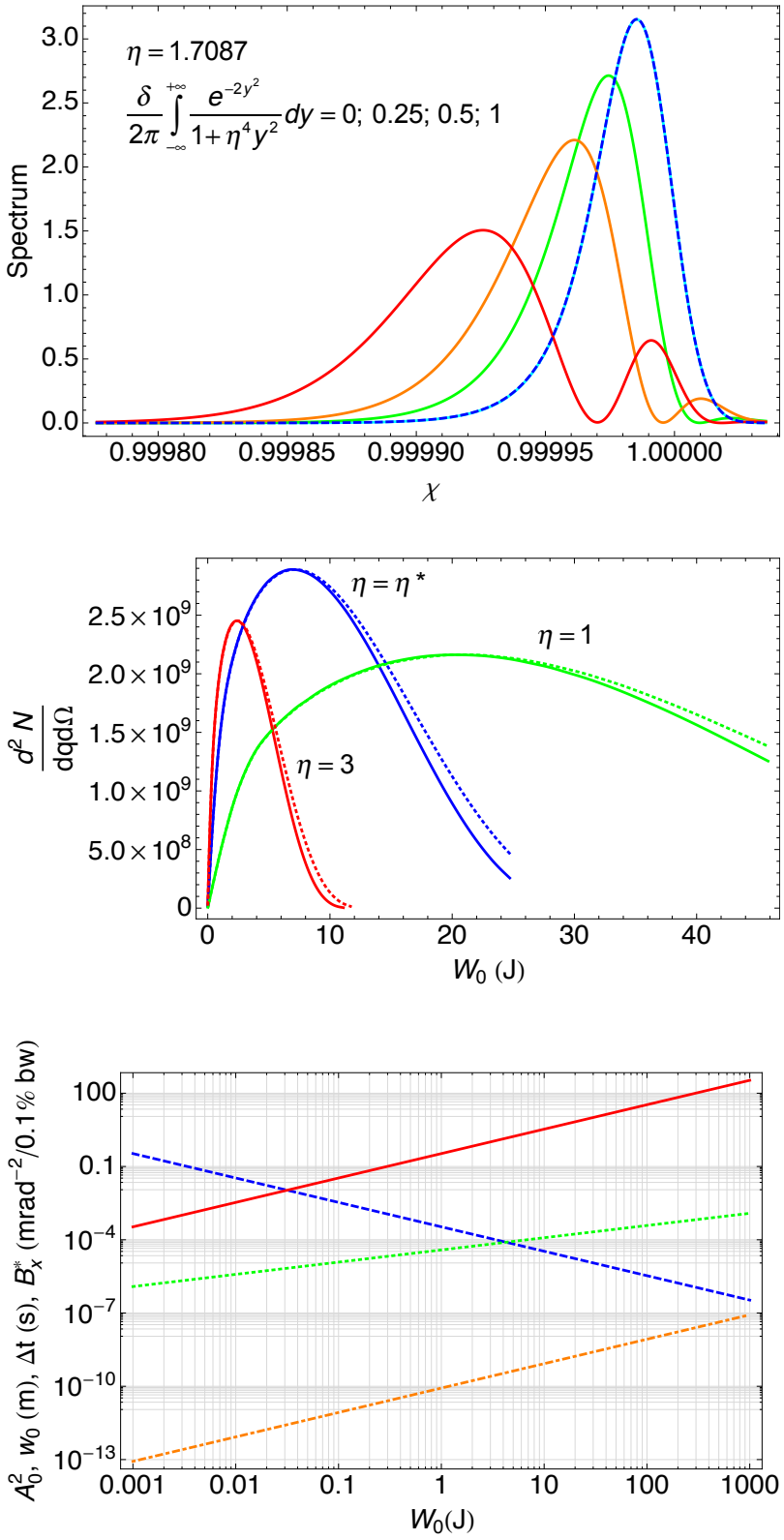
η = 1.7087
δ/2π ∫ e^{-2y^2}/(1+η^4 y^2) dy = 0; 0.25; 0.5; 1
Spectrum
χ
η = η*
η = 1
η = 3
d^2 N/dqdΩ
W0 (J)
A0^2, w0 (m), Δt (s), B*x (mrad^-2/0.1% bw)
W0(J)